

COMMISSIONING OF ELECTRON BEAM DIAGNOSTICS FOR A SRF PHOTOELECTRON INJECTOR

T. Kamps*, D. Böhlick, M. Dirsat, D. Lipka, T. Quast, J. Rudolph, M. Schenk, BESSY, Berlin, Germany
 A. Arnold, F. Staufenbiel, J. Teichert, Forschungszentrum Dresden, Dresden, Germany
 G. Klemz, I. Will, Max Born Institut, Berlin, Germany

Abstract

A superconducting RF (SRF) photoelectron injector is currently under commissioning by a collaboration of BESSY, DESY, FZD and MBI. The project aims at the design and setup of a continuous-wave (CW) SRF electron injector including a diagnostics beamline for the ELBE FEL and to address R&D issues of high brightness CW injectors for future light sources such as the BESSY FEL. The layout and realization of the diagnostics beamline for the electron beam is presented including systems to monitor the momentum, charge, transverse emittance and bunchlength in various operation modes of the injector.

MOTIVATION

Future FEL light sources such as the proposed STARS FEL [1] and the ELBE facility [2] operate with superconducting RF (SRF) for electron acceleration to enable continuous wave (CW) operation generating flexible bunch patterns.

The SRF injector project combines the advantages of photo-assisted production of short electron pulses, high acceleration field at the cathode of an RF field and CW operation of a superconducting cavity. The main challenges are the design of the superconducting cavity with a suitable cathode insertion, the risk of contamination of the cavity with cathode material, and a method to control the transverse emittance of the electron beam. The SRF gun collaboration of BESSY, DESY, FZR and MBI sets out to tackle these issues. The target of the collaboration is to setup a SRF gun [3] together with a diagnostics beamline serving as a test facility for photoelectron injectors. The task of the diagnostics beamline is to ensure safe operation of the injector, check the theoretical model for the injector by measurements and to find an optimum working point for the setup of the injector parameters.

EXPERIMENTAL SETUP

The setup for the photoinjector consists of the SRF gun and the diagnostics beamline as depicted in Fig. 1. The electrons are generated by a pulsed laser beam impinging on the photocathode. The laser is designed to operate at 500 kHz repetition rate delivering pulses of 16 ps FWHM length with 1 μ J pulse energy at 263 nm wavelength [4]. The repetition rate of the laser can be reduced for alignment

and beam diagnostics measurements. This laser serves two operation modes at high bunch charge. A second laser is under development for operation of the injector at higher repetition rate (13 MHz) with a reduced bunch charge of 77 pC. The three main operation modes of the injector are summarized in Tab.1. The photocathode is made of Cs₂Te

	ELBE	HC	FEL
RF frequency		1.3 GHz	
Beam energy		9.5 MeV	
Operation		CW	
Drive laser		263 nm	
Photocathode		Cs ₂ Te	
Pulse length FWHM	5 ps	16 ps	50 ps
Repetition rate	13 MHz	500 kHz	1 kHz
Bunch charge	77 pC	1 nC	2.5 nC
Trans. emittance	1.5 μ m	2.5 μ m	3 μ m

Table 1: Design beam parameters of the three main operation modes: ELBE FEL, at high bunch charge (HC) and BESSY FEL (FEL).

with a quantum efficiency of better than 1 %. This cathode is placed at the entrance of a 3 1/2 cell cavity structure with a RF frequency of 1.3 GHz. The axis peak field of the accelerating mode is 50 MV/m (design value). The cavity structure is embedded in a liquid helium tank. At the exit of the SRF gun the electron beam is focused with a solenoid magnet. After that, the electrons pass the transfer section preparing the beam parameters for injection into the ELBE linac. Behind this section the diagnostics beamline is located, and the beam parameters will be measured.

BEAM CHARACTERIZATION

In order to characterize the performance of the photoinjector, the following beam parameters need to be considered:

- The energy distribution of the beam – the kinetic energy of the electrons and the energy spread. The beam momentum will vary between a few and 9.5 MeV. The minimum momentum spread as expected from simulations will be 36 keV for the low charge operation mode.
- The total beam intensity, together with the time structure. The bunch charge can vary between a few pC

*kamps@bessy.de

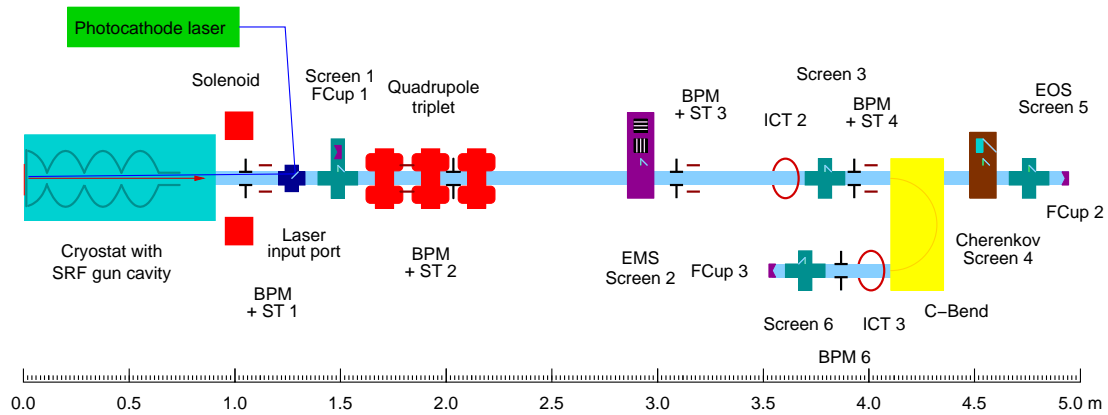


Figure 1: General setup of the SRF gun and diagnostics beamline.

during operation with a Copper cathode and 2.5 nC for nominal operation in the BESSY FEL mode.

- The optical properties, which can be described in terms of the transverse beam emittance. The normalized beam emittance is expected to vary between 1 and 10 mm mrad.

The optical properties are dependent on the intensity and energy distribution of the beam. Therefore all parameters need to be analyzed. In this paper the tools for the characterization of the electron beam are considered.

BEAMLINE OVERVIEW

A schematic overview of the diagnostics beamline and the SRF gun is given in Fig. 1. The diagnostics beamline consists of:

- Six viewscreens for transverse beam profile measurements, marked as Screens 1 to 6 in Fig. 1,
- Five beam position monitors (BPM N) and four steering coil pairs for orbit control (ST M),
- Two integrated current transformers (ICT 1 and 2) to control charge transmission through the beamline,
- One pair of slit masks to analyze the horizontal and vertical beam emittance (EMS),
- One 180 degree dipole spectrometer (C-bend) for momentum and momentum spread measurements,
- A Cherenkov monitor and electro-optical sampling system (EOS) to measure the time structure of the electron pulses, and
- Three Faraday cups, FCup 1 can be inserted at the beginning of the beamline and two (FCup 2 and 3) are included into the beam dumps.

To keep the diagnostics beamline at low pressure (below 10^{-9} mbar), ion vacuum pumps and ion gauges

are mounted below every viewscreen station. For the Cherenkov monitor a differential pumping scheme is applied. Valves are put along the beamline to divide the beamline into different vacuum sectors.

BEAM INTENSITY AND POSITION

Beam Intensity

Faraday cups and integrating current transformers (ICT) are used at several positions to measure the total beam intensity. The Faraday cup is insertable at the location of the first profile monitor port. Two additional Faraday beam dumps are implemented at the dispersive and straight end of the beamline. During commissioning of the beamline average beam currents as low as 50 nA (at 100 kHz repetition rate) have been measured with a sensitive Amperemeter directly connected to the first Faraday cup (FCup1).

Two integrating current transformers [5] are used to continuously monitor the bunch charge at two locations, before and in the dispersive arm of the spectrometer dipole. At low bunch charge and low repetition rate the signal from the ICTs will be amplified by 22 dB using low-noise amplifiers. Tests at the ELBE linear accelerator indicate that bunch charges as low as 10 pC can be resolved with 10% resolution.

Beam Position

The requirements for the beam position measurement are a resolution of better than $100 \mu\text{m}$ for single bunches for beam offsets as far as 5 mm. The readout electronics has to cope with all operation modes. We use stripline BPMs as implemented at the ELBE accelerator. The striplines have a length of $1/4 \lambda_{RF}$ and are mounted in a compact package. The readout electronics utilizes a logarithmic detector for direct RF to DC conversion and a logarithmic amplifier with a large linear dynamic range of 60 dB, the sensitivity of the BPM system is measured to be 0.8 dBm/mm [6].

BEAM PROFILE AND EMITTANCE

Beam Profile

The profile monitors are used to image the full beam at several locations along the beamline and to measure the size of the beamlets released by the emittance measurement slit mask. The relative resolution of the profile monitor has to be better than 10% for full and beamlet imaging. For this purpose thin Yttrium-Aluminum-Garnet (YAG) crystal sheets doped with the visible light scintillator Cerium are inserted into the beam path to produce an image of the transverse charge distribution. This beam image is detected by a CCD camera. The screen material has to be robust and UHV-compatible as the first screen is located in close proximity to the SRF cavity. To provide for the best image fidelity, the screens are mounted at normal incidence to the electron beam. An Aluminum mirror is placed downstream to deflect the fluorescent light out to the camera. Outside the vacuum beam pipe the light is deflected again by a mirror and then focused onto the sensitive area of a CCD camera. The optical focus and magnification can be calibrated by inserting a calibration target at the location of the screen. The minimum object size generated by the crystal screen is dominated by multiple scattering for beam energies below 10 MeV. At 2 to 3 MeV beam momentum the minimum resolution is around $40 \mu\text{m}$ and at 9.5 MeV the resolution is around $10 \mu\text{m}$. During commissioning, the viewscreens were able to withstand operation conditions with several thousand nC per hour without any visible degradation of the beam image. In Fig. 2 the first beam images of the electron beam generated during commissioning are shown.

Emittance Measurement Section

The electron beam generated in the injector is in all nominal operation modes space-charge dominated. For this reason a double slit-based phase space sampling method [7] is considered, where an actuator-mounted slit mask is moved perpendicular across the beam. The purpose of collimating the beam intensity with slits is two-fold. The first is to cut low current beam portions out of the high brightness beam. These small beamlets have the same divergence as the original beam with negligible effects due to space-charge. The second purpose is to separate the beam into many beamlets, whose intensity distribution at some downstream point can be measured to give the phase space distribution of the beam; the width of each beamlet gives a measure of the width of the transverse momentum distribution at each slit, and the centroid of the beamlets gives the correlated offset of the momentum distribution at each slit. The normalized beam emittance can then be calculated according to

$$\epsilon_n = \beta\gamma \sqrt{\langle x^2 \rangle \langle x'^2 \rangle - \langle xx' \rangle^2}. \quad (1)$$

Here $\langle x^2 \rangle$ and $\langle x'^2 \rangle$ are the RMS beam size and divergence of the beam, $\langle xx' \rangle^2$ the correlation between size and divergence and $\beta\gamma$ the relativistic factors.

Facility instrumentation overview

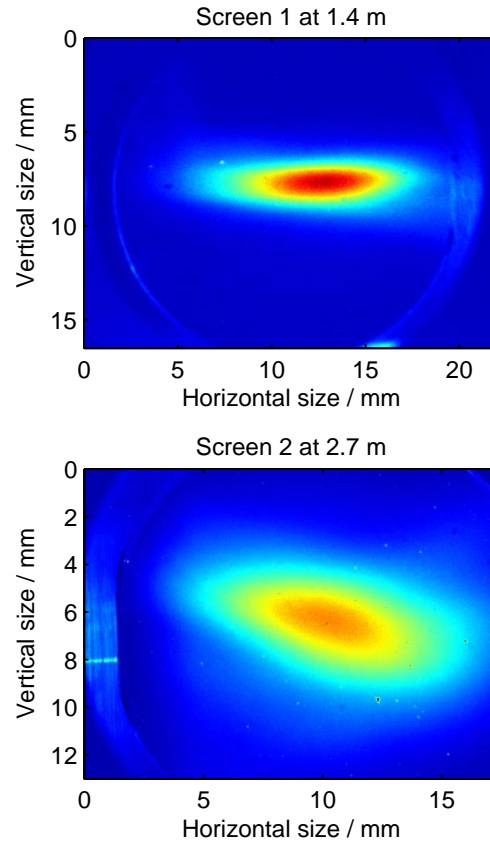


Figure 2: First beam images produced with the electron beam generated by the SRF injector.

The contribution of the slit width towards the beamlet size should be small, but it must be large enough to supply the beamlets with sufficient charge. To meet the requirements of various operation modes, a slitmask with two pairs of slits with $100 \mu\text{m}$ and $50 \mu\text{m}$ width are constructed. For single-shot measurements of the beam emittance, an array with five $100 \mu\text{m}$ slits is also included in the slitmask. The size of the released beamlets will be mea-

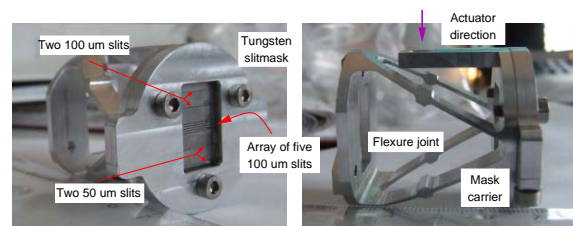


Figure 3: EMS slitmask inside the carrier, which can be tilted with respect to the beam by a flexure joint.

sured with three viewscreen stations downstream in the diagnostics beamline. The stations are located 0.6 m, 1.6 m and 2.0 m after the slit mask. The beamlet sizes at these stations vary between $60 \mu\text{m}$ and $250 \mu\text{m}$. The mask it-

self is made of 1.4 mm thick Tungsten, being an optimum between acceptance and background due to Coulomb scattering. The slits were produced by electro-discharge machining the bulk material with a wire. The material is quite brittle and splinters were found in the slit opening. For this reason the 50 μm slits were produced by sandwiching two polished half-plates. The complete slitmask is placed inside a carrier (see Fig. 3), which can be moved by an actuator inside the beam path. The tilt of the slit mask can be changed by a movable flexure joint. This second actuator is mounted inside the large actuator moving the mask in and out. The size of the individual slits and the spacing of the multi-slit array have been measured by analyzing the Fraunhofer pattern of the slits illuminated by a monochromatic light source. The average slit width for the broad single slits is $d_{sgl} = 85 \pm 2 \mu\text{m}$ and for the slit array $d_{arr} = 84 \pm 8 \mu\text{m}$. The spacing of the slit array is $499 \pm 48 \mu\text{m}$.

TEMPORAL PROFILE

To verify the shape and length of the temporal profile of the electron bunches, two techniques with ps time resolution will be used. Inside the Cherenkov monitor [8] the electron bunches pass a thin sheet of radiator. The radiator emits a Cherenkov radiation pulse with the same time structure as the electron bunch. A streak camera can be used to measure the shape and length of this radiation pulse with ps resolution. This technique is destructive to the electron bunches as the beam size increases during the passage through the radiator. The electro-optic sampling (EOS) diagnostic technique [9] inspects the electric field co-propagating with the electron bunch and enables non-destructive single-shot measurement with sub-ps resolution.

Cherenkov Monitor

The first temporal profile monitor is located after the spectrometer magnet in straight direction. The Cherenkov process is characterized by the Cherenkov-angle $\cos \theta_C = 1/(\beta n)$ (where β is the relativistic velocity factor of the electrons and n the refractive index of the radiator), under which a radiation cone is emitted. The number of emitted photons per pathlength in a bandwidth between wavelength λ_1 and λ_2 is

$$\frac{dN_\gamma}{dx} = 2\pi\alpha z^2 \cdot \sin^2 \theta_C \cdot \frac{\lambda_2 - \lambda_1}{\lambda_1 \lambda_2} \quad (2)$$

where z is the charge in elementary charge units and α the fine-structure constant [10]. Silica aerogel plates of small dimensions with refractive index of $n = 1.008$ and 1.028 are available [11] and considered as Cherenkov radiator. The threshold energy for $n = 1.008$ is 4.1 MeV, for $n = 1.028$ is 2.2 MeV. After emitting Cherenkov radiation, the electron bunch and the light pulse exit the Aerogel plate through a transparent quartz window. The light is then

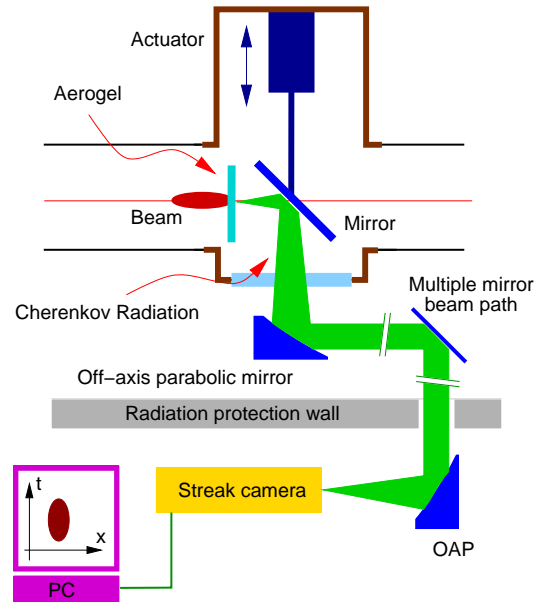


Figure 4: Schematic of the Cherenkov monitor.

reflected by a mirror and leaves the beam pipe through a viewport window (see Fig. 4). The Cherenkov light is then transported with mirrors to the streak camera [12] over a distance of roughly 20 m. The Cherenkov light exits the radiator with large divergence, therefore a relay imaging with focusing elements is necessary to achieve a high photon collection efficiency. Using lenses for this can cause dispersion of the short photon pulse up to several ten picoseconds. Therefore only reflective optical elements, plane and off-axis parabolic mirrors, were considered for the light transport. The setup was simulated with the ray-tracing code RAY [13]. The pulse broadening is dominated by the dispersion in the viewport window, which is $\Delta t = 1.4$ ps for the first viewport and $\Delta t = 3$ ps for the second. Both values are calculated assuming the collection of the wavelength region between 300 and 600 nm. The resolution can be enhanced by limiting the wavelength band with bandpass filters.

Laser Pulse Measurements

First tests with the streak camera were performed to check the laser pulse length and the synchronization of the streak camera to the master oscillator. The intensity of the laser pulses was attenuated by using several low reflectivity optical flats. Synchronization between laser and streak camera is achieved by a 250 MHz PLL synthesizer driven by a 13 MHz reference signal from the laser itself. The synchronization accuracy between laser and streak camera was measured to be better than 2 ps. In Fig. 5 the results for the pulse length measurement are shown. For each data point five streak images were taken. Each image was analyzed by applying a Gaussian fit to the time-projection axis data. The average RMS pulse length for the laser is $\sigma_{t,green} = 6.9 \pm 0.2$ ps and $\sigma_{t,UV} = 6.6 \pm 0.2$ ps. The laser

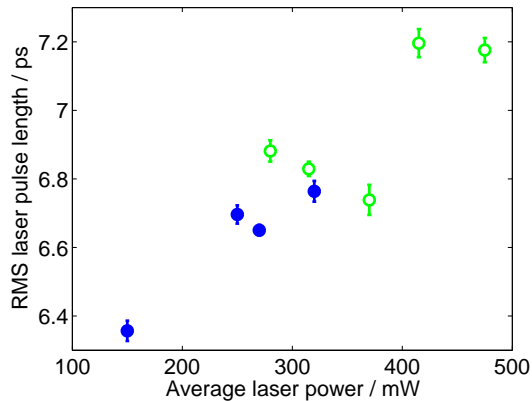


Figure 5: Results from laser pulse length measurements for the green (green and open points) and UV (blue and filled points) output of the laser for different average power levels.

pulse length does not depend on the average laser power. The RMS pulse length of the electron bunches after extraction out of the cathode as measured with a phase scan is $\sigma_e = 7.7 \pm 3.1$ ps.

MOMENTUM AND MOMENTUM SPREAD

The momentum distribution of the electron beam will be measured with a 180° dipole magnet spectrometer. The spectrometer is a H-type dipole with a bending radius of $\rho = 200$ mm and a gap height of $g = 40$ mm. The field map of the magnet has been measured with a hall-probe on a movable stage. By moving the dipole and the hall-probe a two-dimensional map of the field distribution was measured. The relative homogeneity of the field between the pole shoes was measured to be $2.5 \cdot 10^{-4}$, which is below the value specified. A 180° dipole magnet was chosen in order to unfold the contribution of the emittance and Twiss parameter to the beam size measured in the dispersive arm. The deconvolution can be done by putting a second screen in the non-bend plane in a location with the same $|R_{11}|$ and $|R_{12}|$ elements of the transfer matrix [14] as for the bend plane. Such a screen is placed at position of the Cherenkov monitor of the beamline (SC4 in Fig. 1). Simulating the setup with the particle tracking code ASTRA indicates that a momentum spread as low as $\Delta p = 6.3$ keV/c at 10 MeV beam energy and 1 nC bunch charge can be resolved using the setup and the deconvolution technique.

SUMMARY AND OUTLOOK

The diagnostics beamline currently under construction plays a vital role in the commissioning and successful running of the SRF injector. Results from first beam tests at low bunch charge indicate the efficiency of the individual devices.

[Facility instrumentation overview](#)

ACKNOWLEDGMENTS

We want to thank the engineers and technicians from BESSY, FZD and the Max Born Institute who contributed to the SRF injector project. We are grateful by the assistance received by DESY Hamburg and SLAC. We acknowledge the support by the German Federal Ministry of Education and Research Grant 05 ES4BR1/8.

REFERENCES

- [1] M. Abo-Bakr *et al.*, “STARS: A two-stage high-gain harmonic generation FEL demonstrator,” *Prepared for Particle Accelerator Conference (PAC 07), Albuquerque, New Mexico, 25-29 Jun 2007*
- [2] P. Michel *et al.*, “The Rossendorf IR-FEL ELBE,” *Prepared for 28th International Free Electron Laser Conference (FEL 2006), Berlin, Germany, 27 Aug - 1 Sep 2006*
- [3] K. Möller *et al.*, “Development of a superconducting radio frequency photoelectron injector,” *Nucl. Instrum. Meth. A* **577** (2007) 440-454.
- [4] I. Will, G. Klemz, F. Staufienbiel and J. Teichert, “Photocathode laser for the superconducting photo injector at the Forschungszentrum Rossendorf,” *Prepared for 28th International Free Electron Laser Conference (FEL 2006), Berlin, Germany, 27 Aug - 1 Sep 2006*
- [5] Bergoz Instrumentation, “Integrating Current Transformer User’s Manual Rev 3.0,” 2006
- [6] P. Evtushenko, “Electron Beam Diagnostic at the ELBE Free Electron Laser,” PhD thesis, presented at the Technical University Dresden, 2004
- [7] J. Rosenzweig, G. Travish, “Design Considerations for the UCLA PBPL Slit-Based Phase Space Measurement System,” UCLA PBPL Note 1994
- [8] T. Watanabe *et al.*, “Overall comparison of subpicosecond electron beam diagnostics by the polychromator, the interferometer and the femtosecond streak camera,” *Nucl. Instrum. Meth. A* **480** (2002) 315.
- [9] I. Wilke, A. M. MacLeod, W. A. Gillespie, G. Berden, G. M. H. Knippels and A. F. G. van der Meer, “Single-shot electron-beam bunch length measurements,” *Phys. Rev. Lett.* **88** (2002) 124801.
- [10] C. Grupen, “Particle Detectors,” Cambridge University Press (June 28, 1996).
- [11] A. Y. Barnyakov *et al.*, “Development of aerogel Cherenkov detectors at Novosibirsk,” *Nucl. Instrum. Meth. A* **553** (2005) 125.
- [12] Hamamatsu Photonics, “Universal Streak Camera C5680 Series Manual,” 2003
- [13] F. Schäfers, “RAY, the BESSY raytrace program,” BESSY Technical Report TB 202 (96).
- [14] K. L. Brown, “A first and second order matrix theory for the design of beam transport systems and charged particle spectrometers,” *SLAC-R-075, Adv. Part. Phys.* **1** (1968) 71.